This is a preproof accepted article for *Mineralogical Magazine*
This version may be subject to change during the production process
DOI: 10.1180/mgm.2026.10273

Low- and high-temperature evolution of chlorothionite, $K_2Cu(SO_4)Cl_2$

Evgeni V. Nazarchuk[1], Lada R. Zhdanova[1], Oleg I. Siidra[1,2,*]

[1]Department of Crystallography, Saint-Petersburg State University, University emb. 7/9, St. Petersburg 199034, Russia

[2]Kola Science Center, Russian Academy of Sciences, Fersman str. 14, Apatity, Murmansk Region, 184200, Russia

* E-mail: o.siidra@spbu.ru

Abstract

The low- and high-temperature crystal chemistry of chlorothionite, $K_2Cu(SO_4)Cl_2$, a fumarolic copper sulfate-chloride from the Yadovitaya fumarole (Tolbachik volcano, Kamchatka), and its synthetic analogue has been investigated. The study combined in situ single-crystal X-ray diffraction (SCXRD) and powder X-ray diffraction (PXRD). SCXRD measurements were performed over the temperature range 100–700 K, while PXRD data were collected from 300 to 940 K. The synthetic analogue of chlorothionite has recently attracted considerable attention in the fields of solid-state physics and materials science due to its remarkable magnetic properties.

No phase transitions are observed over the entire studied temperature range. However, PXRD reveals that the evolution of the diffraction pattern with increasing temperature can be divided into four distinct stages. Above ~600 K, reflections corresponding to tenorite (CuO) and orthorhombic K_2SO_4 (*Pmcn*) appear in the powder patterns, followed by the formation of hexagonal K_2SO_4 ($P6_3/mmc$) above 680 K. The diffraction peaks of chlorothionite completely disappear after 820 K, leaving tenorite and hexagonal K_2SO_4 as the sole crystalline phases. According to the SCXRD, the thermal expansion of chlorothionite is strongly anisotropic

Prepublished article

throughout the 100–700 K range. Between 100 and 400 K, the expansion is governed by the highly directional thermal response of bond lengths and angles within the coordination polyhedra: the largest expansion occurs along the *b* axis (i.e., along the Cu-polyhedral chains), whereas the *c* axis exhibits negative thermal expansion. Between 400 and 700 K, the expansion along *c* reverses sign, becoming strongly positive; this change is attributed to shear deformations driven by the displacement of potassium atoms. The $[CuCl_2(SO_4)]$ complexes remain essentially rigid upon heating, functioning as stable structural blocks, while the K-O and K-Cl bonds behave as flexible hinges that control the macroscopic thermal response of the framework.

The mineral and its synthetic analogue display virtually identical thermal expansion coefficients. This confirms that trace impurities in the natural sample have no measurable effect on its thermal behavior and validates the use of mineral samples as reliable proxies for the physical properties of their synthetic counterparts.

Keywords: chlorothionite, sulfates, in situ temperature variable single-crystal X-ray diffraction, powder X-ray diffraction, thermal expansion.

1. Introduction

The fumarole fields of the Tolbachik volcano (Kamchatka Peninsula, Russia) have long been a focus of interest across various disciplines in the Earth and materials sciences. The combination of high temperature, atmospheric pressure, elevated oxygen fugacity, the distinctive geochemistry of volcanic exhalations, and a wide spectrum of chalcophile elements gives rise to exceptionally rich mineral assemblages (Vergasova and Filatov, 2012, 2016; Pekov et al., 2020; Borisov et al., 2024). The fumaroles of the Second Cone of the Great Tolbachik Fissure Eruption (GTFE) hold the record for the number of newly discovered mineral species; among the transition metals present there, copper is the most abundant. Several large fumaroles have been documented on the Second Cone, the best known of which

Prepublished article

is the Yadovitaya fumarole (Borisov et al., 2024) with its well-developed sulfate zone. Most anhydrous copper sulfates form and remain stable only under the high-temperature conditions of the fumarole environment. Key factors controlling their stability are temperature and humidity (Siidra et al., 2019), both of which vary with time, either increasing or decreasing. As a result of hydration-driven changes, unique assemblages of secondary hydrated sulfates are produced (Siidra et al., 2014a,b). Some fumaroles that were active decades ago have since disappeared.

Chlorine is an important agent of mass transfer in fumarolic processes (Serafimova, 1979). In the assemblages of the Yadovitaya fumarole, 15 copper chlorides have been identified, four of which are sulfate-chlorides: chlorothionite $K_2Cu(SO_4)Cl_2$ (Giacovazzo and Scordari, 1976), kamchatkite $KCu_3O(SO_4)_2Cl$ (Siidra et al., 2017), nabokoite $KCu_7O(SO_4)_5(TeO_3)Cl$ (Pertlik et al., 1988), and piypite, $K_4Cu_4O_2(SO_4)_4{\cdot}(Na,Cu)Cl$ (Vergasova et al., 1984). Also worth mentioning is the chemically related potassium zinc sulfate-chloride belousovite, $KZn(SO_4)Cl$ (Siidra et al., 2018).

Oxide minerals and oxysalts of divalent copper, Cu^{2+}, provide an important platform for investigating quantum phenomena such as spin-polarised transport, magnetic frustration, spin-liquid behaviour, and spin-canting. The attention of solid-state physicists has been drawn to the family of sulfate-chlorides typified by the mineral chlorothionite. A decade ago, Hälg et al. (2014) investigated the family of spin-chain materials $K_2Cu(SO_4)Cl_2$ and $K_2Cu(SO_4)Br_2$, which are synthetic analogues of chlorothionite and its bromide counterpart, respectively. Bo et al. (2020) calculated the magnetic exchange interactions in these materials. These studies demonstrated that the magnetic subsystem of Cu^{2+} ions in $K_2CuSO_4X_2$ (X = Cl, Br) consists of quasi-one-dimensional spin chains with a dominant superexchange pathway between two Cu^{2+} ions (Pashkov et al., 2024). Similar magnetic behaviour has been observed in the selenate analogues of chlorothionite, $M_2Cu(SeO_4)Cl_2$ (M = K, Rb). A rubidium analogue of

Prepublished article

chlorothionite, $Rb_2Cu(SO_4)Cl_2$, has also been reported (Siidra et al., 2021), although its magnetic properties remain unexplored.

Equally important is an understanding of the mechanisms of thermal expansion and the stability limits of such mineral-like materials (Nazarchuk et al., 2023, 2024). The present paper reports a study of the structural evolution of chlorothionite and its synthetic analogue across a range of temperatures. The thermal expansion of the compounds is examined by a combination of *in situ* single-crystal and powder X-ray diffraction.

2. Materials and Methods

2.1 Materials

The sample, which contains a rich sulfate mineral assemblage including chlorothionite, was collected at a depth of 1.0 m from the Yadovitaya fumarole, Second Scoria Cone, Tolbachik volcano. The mineral is associated with chalcocyanite, euchlorine, chalcanthite, anhydrite, belloite, avdoninite, and eriochalcite. Immediately after recovery, the sample was sealed on-site and kept isolated from the atmosphere. Notably, chlorothionite is quite stable in air under ambient conditions; samples stored without special packaging have remained unchanged for more than 10 years. The mineral does not hydrate in air, retaining both its external shape and crystal structure. Chlorothionite forms lamellar crystals of various blue-green shades with varying intensities up to 500 × 500 × 100 μm (Figure 1).

Prepublished article

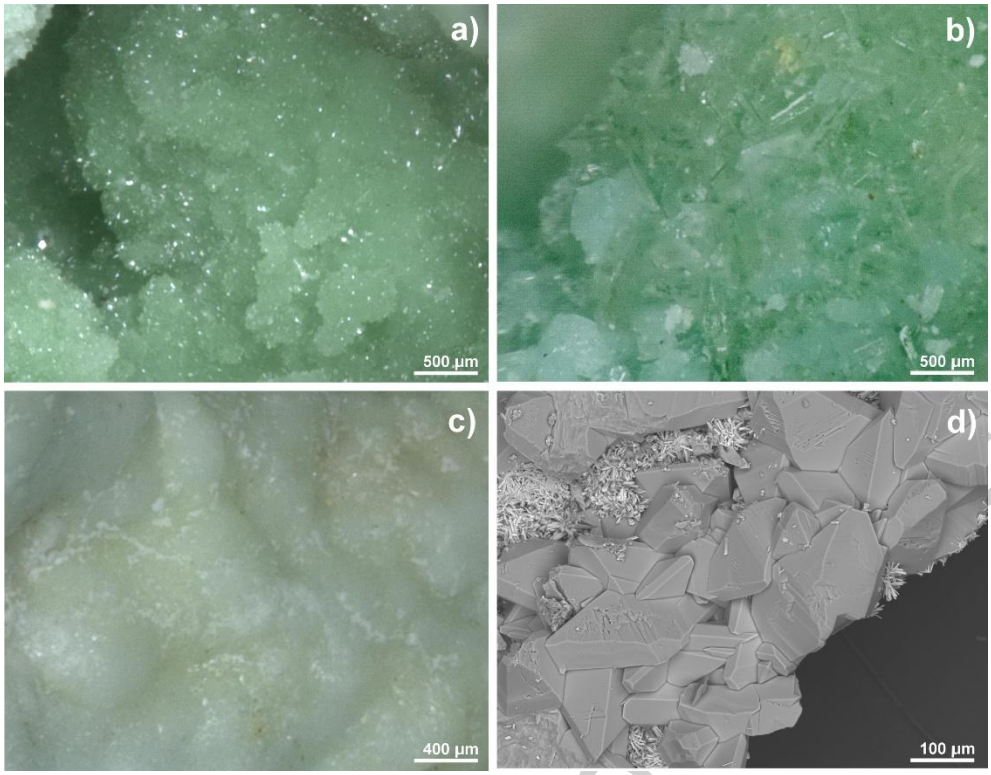


Figure 1. Aggregates of greenish, blue, and blue-gray chlorothionite crystals under the optical microscope (a-c) and a corresponding SEM image (d) showing the crystal morphology. The SEM image was taken from panel (a).

Chemical analyses of chlorothionite were carried out with a Hitachi FlexSEM 1000 scanning electron microscope equipped with an Oxford EDS Xplore Contact 30 detector and the AZtecLive STD analytical system. Analytical conditions were: accelerating voltage 20 kV and beam current 5 nA. The elements K, Cu, S, Cl and O were recorded in all crystals. The elements Na and Mg were detected at concentrations close to the detection limit (Table 1). The color variations are most likely attributable to defects, differences in crystal thickness, and inclusions of anhydrite. No inclusions other than anhydrite were identified. The anhydrite inclusions are irregularly distributed and range in size from a few to several tens of micrometers.

Preprint

Table 1. Chemical composition of differently colored chlorothionite crystals.

	Green		Blue		Blue-gray		
	Wt%	Range	Wt%	Range	Wt%	Range	Probe standard
K_2O	29.91	27.88–30.40	28.95	27.90–30.55	28.64	28.05–29.07	orthoclase
Na_2O	1.12	0.81–1.50	1.39	0.92–1.61	1.55	0.78–2.29	albite
CuO	24.38	23.63–25.06	24.18	23.61–25.46	23.98	22.86–24.04	Cu
MgO	1.20	0.80–1.79	1.50	1.15–2.06	1.67	0.98–1.96	MgO
SO3	26.50	25.12–27.19	26.40	25.02–27.17	26.40	25.93–27.07	baryte
Cl	23.54	22.99–23.85	23.48	23.07–24.02	23.54	22.88–24.08	NaCl
$-O=Cl_2$	-5.32		-5.31		-5.32		
Total	101.33		100.59		100.46		

According to the EMPA results (Table 1), the empirical formulas are $(K_{1.91}Na_{0.11})(Cu_{0.92}Mg_{0.09})(S_{0.99}O_4)Cl_2$, $(K_{1.85}Na_{0.14})(Cu_{0.92}Mg_{0.11})(S_{0.99}O_4)Cl_2$ and $(K_{1.83}Na_{0.15})(Cu_{0.91}Mg_{0.12})(S_{0.99}O_4)Cl_2$ for green, blue, and blue-gray crystals of chlorothionite, respectively.

2.2. Methods

2.2.1 Synthesis

To assess possible differences in thermal behavior and the influence of minor impurities, synthetic analogues of chlorothionite were prepared. All reagents were first dried in an oven at 100 °C for 24 h. A mixture of K_2SO_4, CuO, and KCl in a 1:1:5 molar ratio was briefly ground in air in an agate mortar and placed in a quartz tube that had been sealed at one end. The total mass of the charge was 0.5 g. The quartz tube (6 mm inner diameter, 2 mm wall thickness, 10 cm long) was evacuated with a pump and sealed with a burner flame. The sealed tube was placed in a tube furnace and heated to 600 °C at a rate of 50 °C h^{-1}, held at that temperature for 90 h, and then cooled to room temperature at 20 °C h^{-1}. Well-formed crystals of $K_2Cu(SO_4)Cl_2$ grew on the inner walls of the tube. A conglomerate of $K_2Cu(SO_4)Cl_2$ and anhydrous $CuSO_4$ crystals also formed inside the tube. Bluish-gray crystals of synthetic chlorothionite form intergrowths; the crystal dimensions do not exceed 0.09 × 0.07 × 0.08 mm. In small cleavage fragments, the crystals are transparent and free of visible defects.

Prepublished article

2.2.2 Low temperature and high temperature single-crystal X-ray diffraction (LT-SCXRD and HT-SCXRD).

Single-crystal X-ray diffraction data for chlorothionite and its synthetic analogue were collected on a Rigaku XtaLAB Synergy-S diffractometer equipped with a PhotonJet-S detector and operated with Mo*K*α radiation (50 kV, 1 mA). A suitable single crystal was selected, and more than a hemisphere of data was recorded with a frame width of 0.5° in ω and an exposure time of 10 s per frame. Data integration and absorption correction (multi-scan) were performed using the Rigaku Oxford Diffraction CrysAlis Pro software (version 171.41.86a).

Chlorothionite and its synthetic analogue crystallize in the orthorhombic space group *Pnma*. The difference in the unit-cell parameters does not exceed 0.015 Å (*a* = 7.7065(3) and 7.6931(4) Å, *b* = 6.0177(3) and 6.0180(4) Å, *c* = 16.3165(6) and 16.3181(9) Å, *V* = 756.68(6) and 755.48(7) Å^3 for the mineral and its synthetic analogue, respectively). Natural and synthetic chlorothionite crystals were each studied over the temperature range 100-400 K using a Cobra Oxford CryoSystem and over the range 400-700 K using a Hot Air Gas Blower. In the first interval, the temperature step was 10 K; in the second, 25 K. For the low-temperature measurements, the crystal was glued to a quartz fiber, whereas for the high-temperature measurements it was placed in a quartz capillary. In both cases, the crystal was thermostated before each data collection. Temporal restrictions and the significant reduction in reflection intensities caused by extinction from the capillary walls meant that fewer data collections could be performed in the high-temperature interval. All structures were refined with the SHELX software package (Sheldrick, 2015), starting from the atomic coordinates reported by Giacovazzo and Scordari (1976). Atomic coordinates and displacement parameters for each temperature are given in the corresponding CIF; crystallographic parameters for the mineral sample for selected temperatures are listed in Table 2.

Prepublished article

Table 2. Crystallographic data and refinement parameters for chlorotionite from the Yadovitaya fumarole.

Temperature, K	100	200	300	400	500	600
Radiation	Mo*Kα*, 0.71073 Å					
Crystal system	orthorhombic					
Space group	*Pnma*					
a (Å)	7.7065(3)	7.7152(4)	7.7316(4)	7.7494(4)	7.7599(4)	7.7845(5)
b (Å)	6.0177(3)	6.0458(3)	6.0799(3)	6.1136(4)	6.1287(4)	6.1537(4)
c (Å)	16.3165(6)	16.3163(9)	16.3021(9)	16.2918(10)	16.2884(9)	16.3232(11)
Volume (Å^3)	756.68(6)	761.07(7)	766.32(7)	771.85(8)	774.64(7)	781.94(9)
d_{calc} (g/cm^3)	2.728	2.712	2.693	2.674	2.664	2.640
μ (mm^{-1})	4.917	4.889	4.855	4.821	4.803	4.758
Crystal size (mm)	0.09 × 0.08× 0.06					
θ range (°)	3.609-27.999	3.594-27.994	3.577-27.991	3.559-27.989	3.552-27.997	3.538-27.996
h, *k*, *l* ranges	–8 →10, –7 →7, –21 →18	–10 →9, –7 →7, –20 →21	–10 →9, –8 →7, –21 →20	–9 →10, –8 →7, –20 →21	–10 →10, –8 →5, –20 →21	–10 →10, –8 →5, –20 →21
Total reflections collected	991	973	977	983	1013	1023
R_{int}	0.016	0.016	0.015	0.016	0.029	0.025
$R_1[F > 4\sigma F]$, $wR_2[F > 4\sigma F]$	0.018, 0.049	0.019, 0.053	0.026, 0.070	0.038, 0.109	0.047, 0.130	0.049, 0.153
R_{all}, wR_{all}	0.019,	0.022,	0.029,	0.043,	0.065,	0.066,

Prepublished article

	0.049	0.055	0.072	0.115	0.146	0.049
Goodness-of-fit	1.083	1.094	1.103	1.076	1.071	1.168

2.2.3 High-temperature powder X-ray diffraction (HT-PXRD)

This study was performed on a natural mineral sample. The mineral sample was suspended in dry heptane and deposited onto a Pt–Rh holder. Variable-temperature powder X-ray diffraction patterns were recorded on a Rigaku Ultima IV diffractometer equipped with a Rigaku HTA-1600 camera (low vacuum of 600 Pa), Co *K*α radiation, and a linear PSD detector over the temperature range 300-940 K (20 K step). The heating rate was 2 K min^{-1}. Phase identification was carried out using the PDF-2 database (International Centre for Diffraction Data, http://www.icdd.com/, accessed 2020) and the PDXL and TOPAS V.5.0 (Bruker-AXS 2014) software.

3. Results

3.1. Crystal structure of chlorothionite at 100K

The crystal structures of the mineral and its synthetic analogue are identical. Therefore, all subsequent details are described using a crystal from the natural mineral sample. The crystal structure of chlorothionite contains one symmetrically independent Cu atom and two independent K atoms (Figure 2a). The Cu atom is coordinated by two O atoms (<Cu–O> = 2.013 Å) and four Cl atoms (<Cu–Cl> = 2.246 and 3.015 Å), forming a [4+2]-distorted CuO_2Cl_4 octahedron (Bersurker, 1984)). The K1 atom is surrounded by six O atoms (<K1–O> = 2.703 and 3.309 Å) and two Cl atoms (<K1–Cl> = 3.191 Å), defining a distorted $K1O_6Cl_2$ polyhedron. The K2 atom is coordinated by four O atoms (<K2–O> = 2.797 Å) and four Cl atoms (<K2–Cl> = 3.149 Å), giving a distorted $K2O_4Cl_4$ polyhedron. A single symmetrically unique S atom is tetrahedrally coordinated by four O atoms (Figure 2b), with <S–O> = 1.485 Å.

Prepublished article

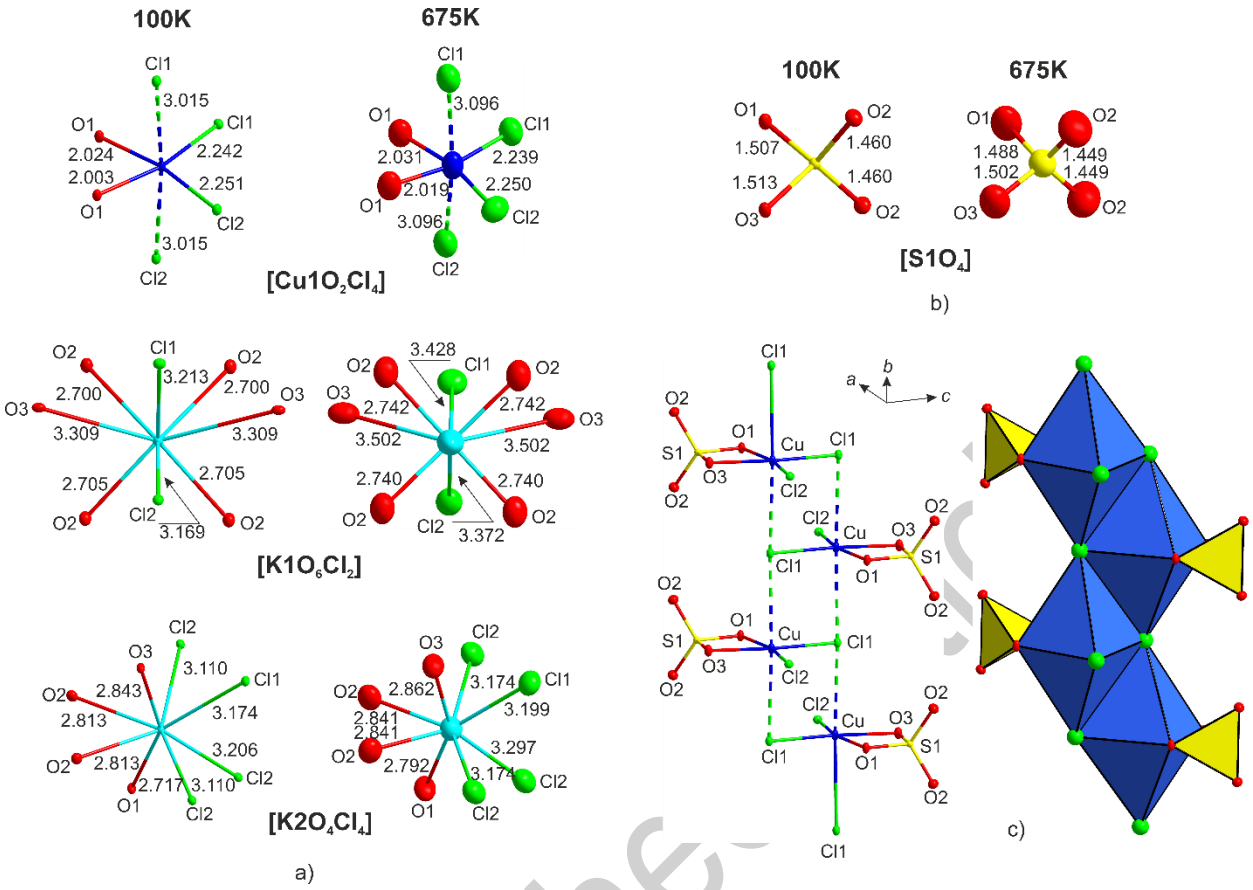


Figure 2. Coordination environments of the cations in the structure of chlorothionite (a-b). Chains of Cu-centred polyhedra decorated by SO_4 tetrahedra (c).

Bond-valence sums for Cu–O, K–O and S–O were calculated using the parameters of Gagné and Hawthorne (2015), whereas those for Cu–Cl and K–Cl were calculated using the parameters of Brese and O'Keeffe (1991) and Brown and Altermatt (1985), respectively. The resulting total bond-valence sums, 1.95, 1.13, 1.19 and 5.81 valence units for Cu, K1, K2 and S1, respectively, are in good agreement with the formal valences of the atoms (Table 3).

Prepublished

Table 3. The bond-valence sums for the atoms in the structure of chlorothionite at 100 K.

	O1	**O2**	**O3**	**Cl1**	**Cl2**	
Cu	0.41		0.39	$0.52+0.06^{\times 2}$	0.51	**1.95**
K1		$0.19^{\times 4}$	$0.04^{\times 2}$	0.13	0.14	**1.13**
K2	0.19	$0.15^{\times 2}$	0.14	0.14	$0.16^{\times 2}+0.13$	**1.19**
S1	1.37	$1.54^{\times 2}$	1.35			**5.81**
	1.97	**2.07**	**1.92**	**0.91**	**0.94**	

The chlorothionite structure is built from rod-like chains (Figure 2c). The chains consist of CuO_2Cl_4 polyhedra connected by sharing Cl1–Cl1 edges. The chains are decorated by SO_4 tetrahedra running parallel to the *b* axis. Potassium atoms are located between the chains and link them into a framework (Figure 3). This arrangement creates a series of soft hinges: Cl2–K1–Cl1, O2–K1–Cl1, O2–K1–Cl2, and O2–K1–O2. Notably, the K1–Cl2 (3.168 Å), K1–Cl1 (3.213 Å) and K1–O3 (3.309 Å) distances between the potassium atoms and the Cu-polyhedral chains are nearly 0.5 Å longer than the K1–O2 bonds (2.706 Å) within the chains.

3.2. Crystal structure evolution upon heating.

No phase transitions were detected over the entire temperature range investigated by low- and high-temperature X-ray diffraction, either for chlorothionite or for its synthetic analogue. According to the SCXRD, the mineral and its synthetic counterpart exhibit essentially identical thermal behaviour. Both compounds are stable up to 675 ± 10 K (~ 400 °C); above this temperature the single-crystal diffraction spots disappear. The loss of crystallinity is accompanied by a color change of the crystal from colorless to black. After subsequent cooling to 300 K, the crystal remains X-ray amorphous.

Prepublished article

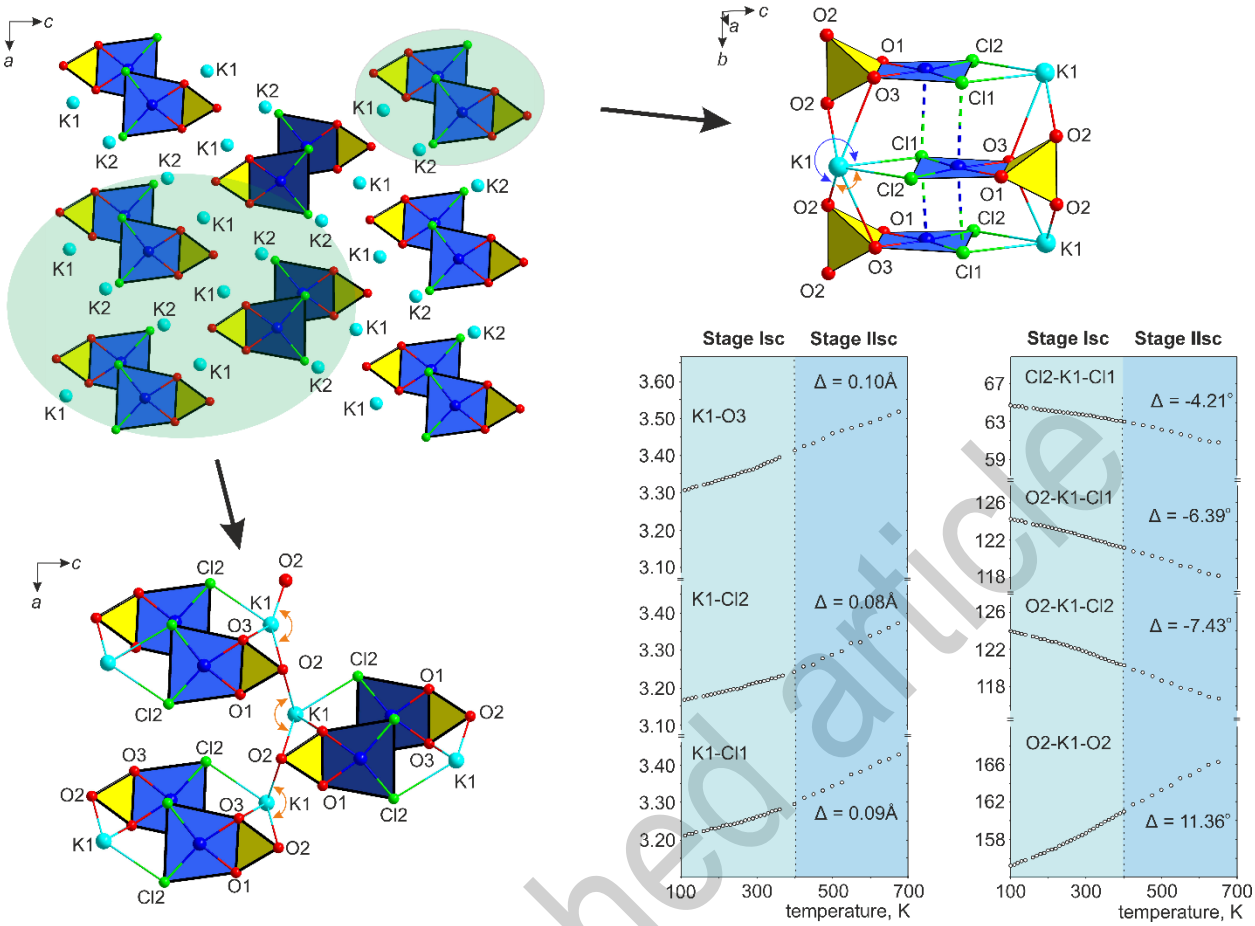
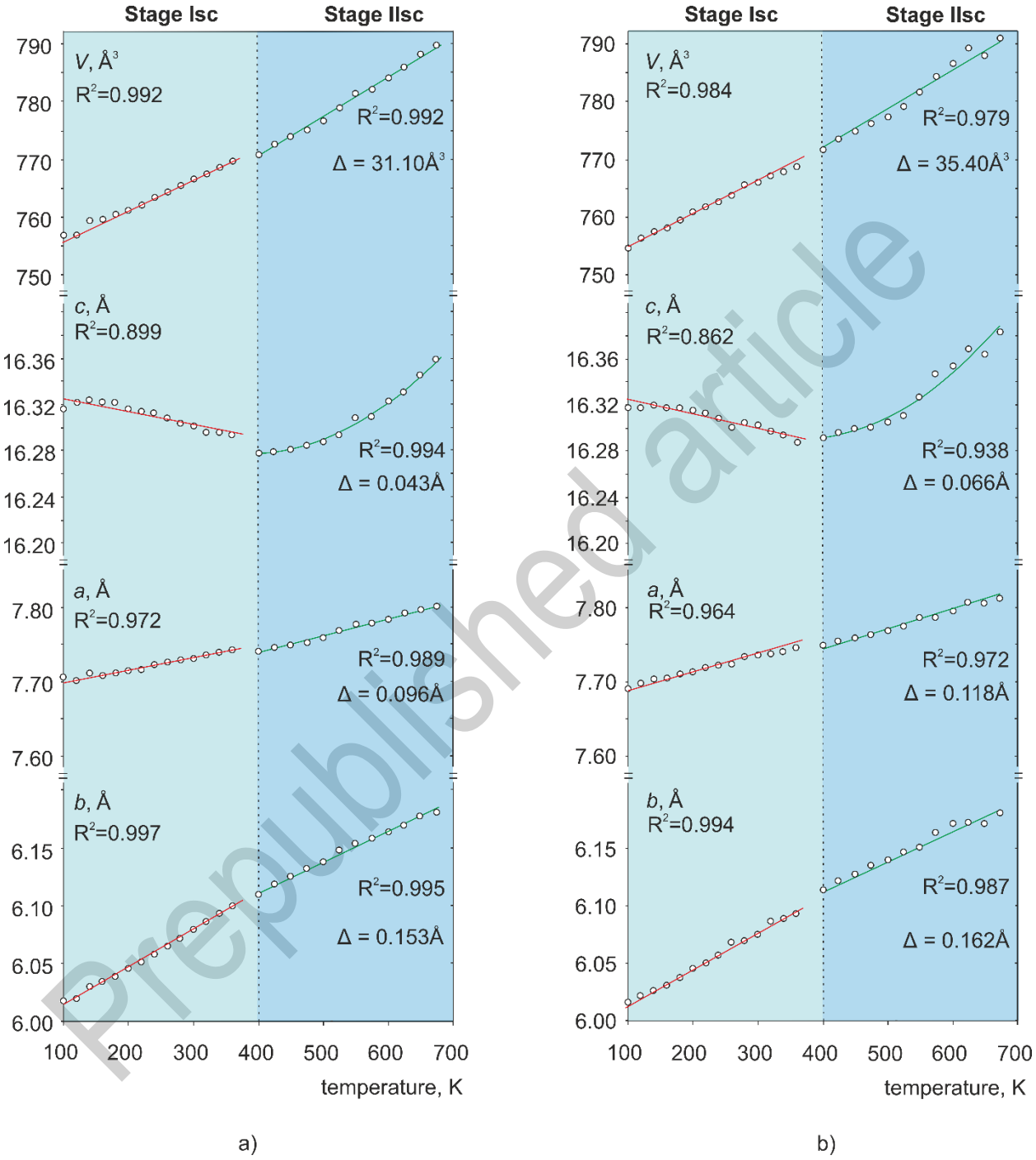


Figure 3. Projection of the crystal structure of chlorothionite onto the *ac* plane (top left). An enlarged fragment showing the flexible K–O and K–Cl bonds and the corresponding angles is given on the right. The O2–K1–O2 angles are shown by the red arrows at bottom left. Evolution of the most temperature-sensitive K–Cl and K–O bond lengths, and of the Cl–K–Cl, O–K–Cl and O–K–O angles, upon heating (bottom right).

The thermal evolution of the unit-cell parameters of chlorothionite and its synthetic analogue over the 100–700 K range is presented in Figure 4. For both compounds, the *a* and *b* parameters and the unit-cell volume *V* increase with rising temperature. The *c* parameter displays two distinct regimes (denoted **Stage Isc** and **Stage IIsc;** sc = single-crystal): 100–370 K and 380–700 K. In **Stage Isc**, *c* decreases slightly, whereas in **Stage IIsc** it increases following a hyperbolic trend. The temperature dependences of *a*, *b*, and *V* are well described

Prepublished article

by first-degree polynomials over both intervals. The *c* parameter also shows a linear dependence in the first interval, but a polynomial dependence in the second.



Prepublished article

Figure 4. Evolution of the unit-cell parameters of (a) chlorothionite and (b) its synthetic analogue upon heating from 100 to 700 K, obtained by *in situ* single-crystal X-ray diffraction. In the 100-400 K interval, half of the data points corresponding to the measurements performed were omitted for clarity.

The temperature dependences of the unit-cell parameters are closely similar for chlorothionite and its synthetic analogue (Figure 4), and can be regarded as essentially identical over both intervals. Between 100 and 700 K, the *a* and *b* parameters exhibit the largest increases: *a* expands by 0.09 and 0.12 Å, and *b* by 0.15 and 0.16 Å, for the mineral and its synthetic counterpart, respectively. In the **Stage Isc**, the *c* parameter contracts slightly (–0.025 and –0.019 Å), whereas in the **Stage IIsc** it expands (0.081 and 0.087 Å) by amounts comparable to those observed for *a* and *b*.

The thermal expansion of chlorothionite is strongly anisotropic over both temperature intervals. In the **Stage Isc**, the largest expansion occurs along the *b* axis (α_{22} = 49.5(1) × 10^{-6} K^{-1}). Expansion along the *a* axis is more than two time smaller (α_{11} = 26.82(7) × 10^{-6} K^{-1}), whereas along the *c* axis the structure undergoes contraction (α_{33} = -20.7(3) × 10^{-6} K^{-1}). It is noteworthy that the thermal expansion coefficients remain essentially constant over the 100–400 K interval.

Over the **Stage IIsc**, the coefficients along the *a* and *b* axes remain nearly constant (α_{11} = 26.43(7) × 10^{-6} K^{-1}; α_{22} = 48.1(1) × 10^{-6} K^{-1}) and are comparable to those observed at lower temperatures. In striking contrast, the expansion along c reverses sign and becomes positive, with α_{33} changing from -20.7(3) to 29.2(2) × 10^{-6} K^{-1} - an increase of more than a factor of three. The volumetric coefficient α_V remains nearly constant between 100 and 400 K (55.6(2) × 10^{-6} K^{-1}), but by 700 K it has grown by roughly 50 % to 103.8(2) × 10^{-6} K^{-1}.

As temperature rises, the character of the expansion evolves in a way that points to pronounced shear deformations. Throughout the 100–700 K interval, chlorothionite displays strongly anisotropic thermal expansion, which originates from the highly directional thermal response of bond lengths and angles within the coordination polyhedra. Most bond lengths change by no more than 0.03 Å; the few that deviate from this pattern are K1–Cl2 (0.08 Å), K1–Cl1 (0.09 Å) and K1–O3 (0.10 Å).

Prepublished article

The sharing of vertices between the K- and Cu-centred polyhedra and the SO_4 tetrahedra generates a set of flexible hinges within the framework (Figure 2). Over the full temperature range, the majority of angles vary by less than 2°. The only substantial angular changes occur at the hinge linkages: Cl2–K1–Cl1 (Δ = –4.21°), O2–K1–Cl1 (Δ = –6.39°), O2–K1–Cl2 (Δ = –7.43°) and O2–K1–O2 (Δ = 11.36°).

3.3. HT-PXRD and decomposition of chlorothionite

The polycrystalline aggregate of chlorothionite is stable up to 600 ± 20 K (Figure 5). The evolution of its diffraction pattern with increasing temperature can be divided into four stages (**Stage Ip – Stage IVp**; p = powder). In **Stage Ip** (300–580 K), only peaks belonging to chlorothionite are present. In **Stage IIp** (580–660 K), peaks of tenorite, CuO and orthorhombic K_2SO_4 (*Pmcn*) appear alongside those of the mineral. At 680 K, peaks of hexagonal K_2SO_4 ($P6_3/mmc$) also emerge. All four phases coexist up to 800 K (**Stage IIIp**). At 820 K, the peaks of chlorothionite and orthorhombic K_2SO_4 disappear completely. **Stage IVp** (820–940 K) is characterized solely by peaks of K_2SO_4 ($P6_3/mmc$) and tenorite. Further heating leads to amorphization of the sample.

Prepublished article

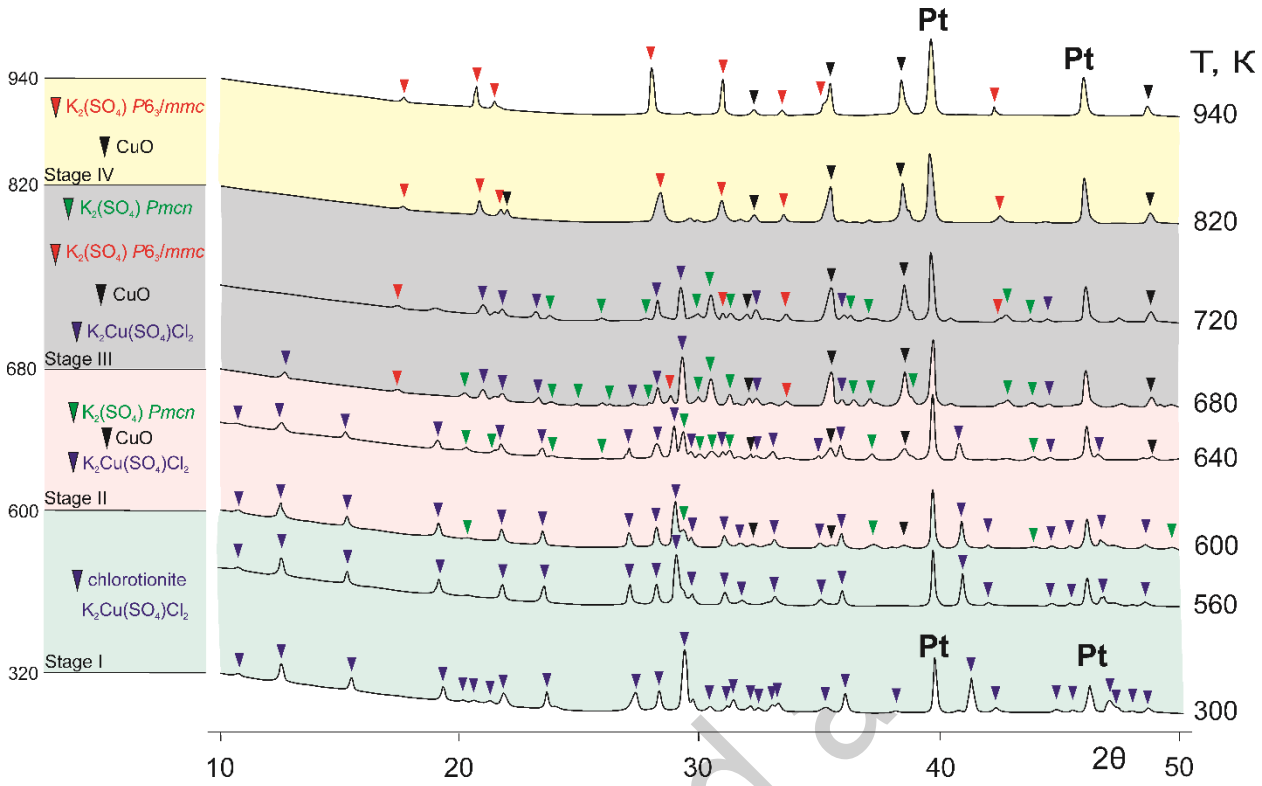


Figure 5. Evolution of polycrystalline chlorothionite upon heating, showing powder X-ray diffraction patterns as a function of temperature (300–940 K).

4. Discussion

The thermal expansion coefficients obtained for chlorothionite and its synthetic analogue are in close agreement (Table 4). Over the 100–700 K temperature interval, α_{11} and α_{22} remain virtually unchanged, whereas α_{33}, and consequently α_V, vary considerably. The largest thermal expansion occurs along the *b* axis, which coincides with the direction of the chains formed by edge-sharing Cu-centred polyhedra (Figures 2, 3). Owing to the Jahn–Teller effect, the Cu-polyhedral chains exhibit strongly anisotropic bond lengths. Each Cu polyhedron consists of a CuO_2Cl_2 square plane complemented by two very long Cu-Cl bonds. The equatorial Cu–Cl distances are 0.768 Å shorter than the axial ones. Over the 100–700 K range, the equatorial Cu–Cl bond lengths remain essentially unchanged, whereas the axial bonds lengthen by 0.082 Å. Such behavior is typical of Jahn–Teller-distorted Cu polyhedra (Bersuker, 1984).

Prepublished a

Table 4. Thermal expansion coefficients for chlorothionite mineral sample and its synthetic analogue over the 100–700 K range.

	Chlorotionite mineral sample	Synthetic analogue
Temperature range	100–700 K	100–700 K
α_{11} ($\times 10^{-6} K^{-1}$)	26.82(71) → 26.43(70)	22.21(94) → 21.94(93)
α_{22} ($\times 10^{-6} K^{-1}$)	49.5(1.2) → 48.1(1.1)	44.5(1.2) → 43.4(1.2)
α_{33} ($\times 10^{-6} K^{-1}$)	-20.7(2.8) → 29.2(2.5)	-20.1(3.8) → 21.7(3.3)
α_V ($\times 10^{-6} K^{-1}$)	55.6(2.1) → 103.8(2)	46.6(2.5) → 87.0(2.4)

The most pronounced variation in thermal expansion is observed along the *c* axis (Table 3). Notably, the positions of the [$(CuCl_2)(SO_4)$] complexes remain virtually unaltered upon heating (Figure 6). In contrast, the positions of the K atoms change: the K2–K2 distance increases (6.351 and 6.382 Å at 100 and 675 K, respectively), whereas the K1–K1 distance decreases (4.022 and 3.952 Å at 100 and 675 K, respectively).

Prepublished article

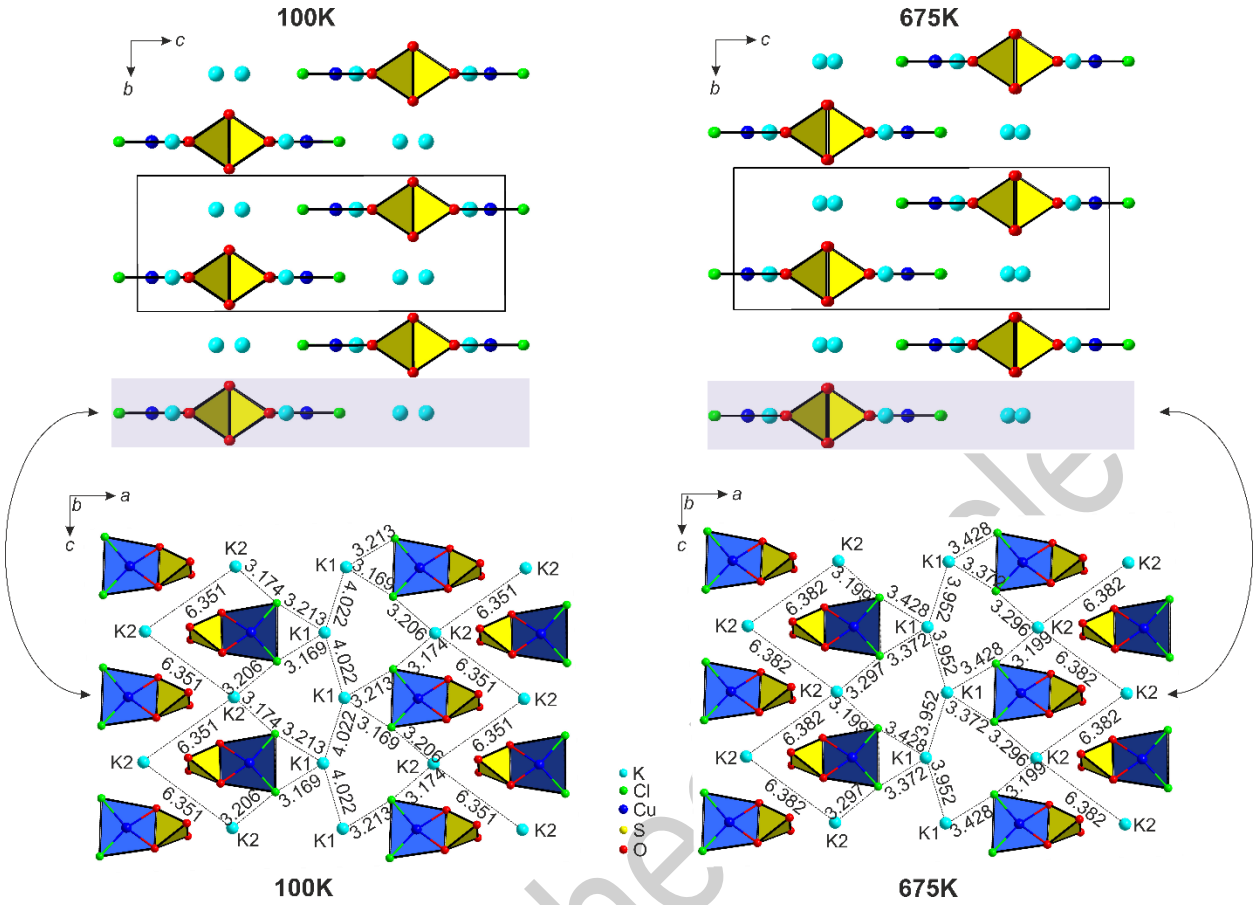


Figure 6. Thermal evolution of chlorothionite. Projections of the crystal structure onto the *bc* and *ac* planes at 100 K (left) and 675 K (right). Dashed lines indicate distances between potassium atoms; the most significant changes in K–K distances are highlighted in red circles.

In the chlorothionite structure, all atoms except O2 occupy special positions whose coordinates are fixed along the *b* axis. Upon heating from 100 to 675 K, the *x* coordinates also change by no more than 0.005 Å. In contrast, significant displacements are observed for the *z* coordinates (Figure 7). The K1 atom shifts three times as far along *z* (–0.016 Å) as along *x*. The K2 and Cl atoms exhibit their largest shifts along z up to 400 K, but by 675 K their coordinates nearly return to their initial values. This behavior correlates well with the temperature dependence of the *c* parameter.

Prepublished

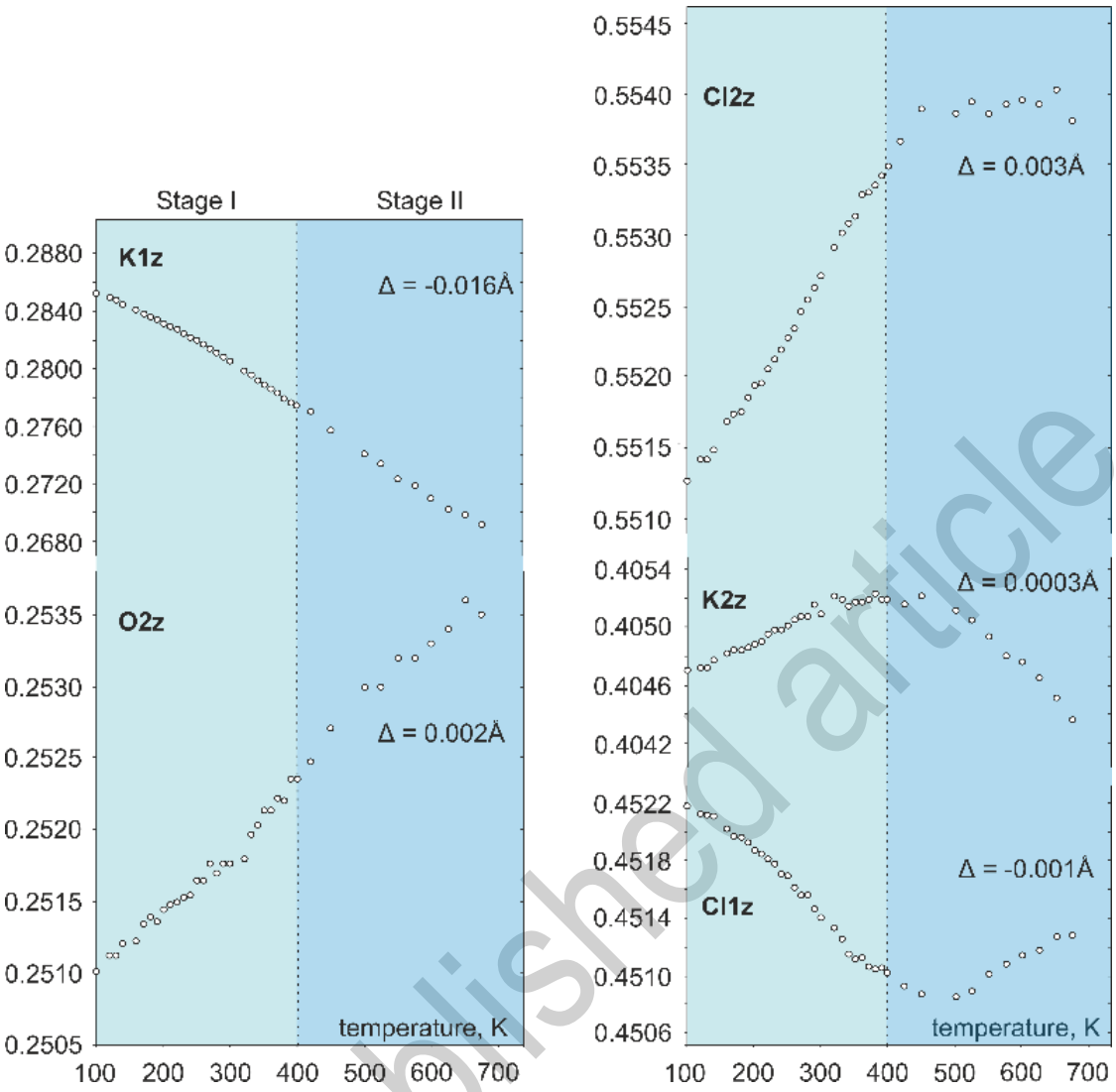


Figure 7. Evolution of the atomic z coordinates in the crystal structure of chlorothionite upon heating from 100 to 700 K, obtained by *in situ* single-crystal X-ray diffraction.

Concluding remarks

The thermal evolution of chlorothionite, and its synthetic analogue has been characterized in detail by a combination of *in situ* single-crystal and powder X-ray diffraction over the temperature range 100–700 K. The following conclusions can be drawn:

i). The crystal structure of chlorothionite, built from Jahn-Teller-distorted copper polyhedral chains decorated by SO_4 tetrahedra and linked by potassium atoms, displays a strongly anisotropic thermal expansion. The largest expansion occurs along the *b* axis, which coincides with the elongation direction of the chains.

Prepublished article

ii). The thermal expansion along the *c* axis exhibits an unusual behaviour: it is negative below ~400 K and becomes positive above this temperature.

iii). The mineral and its synthetic analogue show virtually identical thermal behaviour, confirming that the minor chemical impurities present in the natural sample have no measurable effect on the thermal expansion. This close correspondence validates the use of mineral samples in physical property studies and, in certain cases, allows the properties determined on natural crystals to be directly extrapolated to their synthetic materials, thereby accelerating the characterisation of such systems without the need for time-consuming synthesis optimization.

iv). The overall thermal evolution of chlorothionite is broadly similar to that of other anhydrous copper sulfates from Tolbachik fumaroles, such as piypite and kamchatkite. Upon heating, the mineral gradually loses chlorine and decomposes to form tenorite, CuO and K_2SO_4. The decomposition onset temperature is also similar.

v). The *in situ* single-crystal X-ray diffraction study reveals that the $[(CuCl_2)(SO_4)]$ complexes remain essentially rigid over the entire temperature range, acting as stable structural blocks. In contrast, the potassium atoms serve as flexible hinges whose mobility governs the macroscopic thermal response of the framework.

These results provide a comprehensive description of the thermal behaviour of chlorothionite and establish a foundation for future studies of the stability and compatibility of this family of compounds in potential functional applications.

Prepublished article

Acknowledgements

This work was financially supported by the Russian Science Foundation through the grant 25-17-00157. Technical support by the X-Ray Diffraction Resource Center of Saint-Petersburg State University is gratefully acknowledged.

Reference

Bersuker, I.B. (1984) Jahn-Teller effect and vibronic interactions in modern chemistry. Springer New York, 319 pp. https://doi.org/10.1007/978-1-4613-2653-3

Bo, X., Wang, D., Wan, B. and Wan, X.G. (2020) Calculated magnetic exchange interactions in the quantum spin chain materials $K_2Cu(SO_4)Cl_2$ and $K_2Cu(SO_4)Br_2$. *Physical Review B*, **101**, 024416. https://doi.org/10.1103/PhysRevB.101.024416

Borisov, A.S., Siidra, O.I., Vlasenko, N.S., Platonova N.V., Schuldt Th., Neuman M., Strauss H. and Holzheid, A. (2024) The Yadovitaya fumarole, Tolbachik volcano: A comprehensive mineralogical and geochemical study and driving factors for mineral diversity. *Geochemistry*, **84**, 126179. https://doi.org/10.1016/j.chemer.2024.126179

Brese, N.E. and O'Keeffe, M. (1991) Bond-valence parameters for solids. *Acta Crystallographica* **B47**, 192-197. https://doi.org/10.1107/S0108768190011041

Brown, I.D. and Altermatt, D. (1985) Bond-valence parameters obtained from a systematic analysis of the inorganic crystal structure database. *Acta Crystallographica*, **B41**, 244-247

Bubnova, R.S., Firsova, V.A. and Filatov, S.K. (2013) Software for determining the thermal expansion tensor and the graphic representation of its characteristic surface (theta to tensor-TTT). *Journal of Physical Chemistry of Glasses*, **39**, 347–350. https://doi.org/10.1134/S108765961303005X

Gagné, O.C. Hawthorne F.C. (2015) Comprehensive derivation of bond-valence parameters for ion pairs involving oxygen. *Acta Crystallographica*, **B71**, 562-578. DOI: 10.1107/S2052520615016297

Giacovazzo, C. and Scordari, F. (1976) The crystal structure of chlorotionite, $CuK_2Cl_2SO_4$. *Zeitschrift für Kristallographie*, **144**, 226–237.

Preprinted article

Hälg, M., Lorenz, W.E.A., Povarov, K.Yu., Månsson, M., Skourski, Y. and Zheludev, A. (2014) Quantum spin chains with frustration due to Dzyaloshinskii-Moriya interactions. *Physical Review B*, **90**, 174413. https://doi.org/10.1103/PhysRevB.90.174413

Nazarchuk, E.V., Siidra, O.I., Filatov, S.K., Charkin, D.O. and Zhdanova, L.R. (2023) Thermal expansion of anhydrous copper sulfate minerals determined by single crystal X-ray diffraction: chalcocyanite $CuSO_4$, dolerophanite Cu_2OSO_4 and kamchatkite $KCu_3O(SO_4)_2Cl$. *Physics and Chemistry of Minerals*, **50**. https://doi.org/10.1007/s00269-023-01236-7

Nazarchuk, E.V., Siidra, O.I., Charkin, D.O., Nikolaevich, G.V., Borisov, A.S. and Ugolkov, V.L. (2024) Vergasovaite to cupromolybdite topotactic transformation with crystal shape preservation. *American Mineralogist*, **109**, 471–481. https://doi.org/10.2138/am-2022-8753

Pashkov, G., Markina, M., Lyssenko, K. and Berdonosov, P. (2024) Synthesis, crystal structure, and thermodynamic properties of two new selenate chlorides: $M_2Cu(SeO_4)Cl_2$ with M = K and Rb. *Materials Chemistry and Physics*, **319**, 129367. https://doi.org/10.1016/j.matchemphys.2024.129367

Pekov, I.V., Zubkova, N.V., Koshlyakova, N.N., Shchipalkina, N.V., Sandalov, F.D., Yapaskurt, V.O., Turchkova, A.G., Agakhanov, A.A. and Sidorov, E.G. (2020) Oxidizing-type fumaroles of the Tolbachik volcano, a mineralogical and geochemical unique. *Russian Geology and Geophysics*, **61**, 675–688. https://doi.org/10.15372/RGG2019167

Pertlik, F. and Zemann, J. (1988) The crystal structure of nabokoite, $Cu_7TeO_4(SO_4)_5Cl$: The first example of a $Te(IV)O_4$ pyramid with exactly tetragonal symmetry. *Mineralogy and Petrology*, **38**, 291–298. https://doi.org/10.1007/BF01167095

Serafimova, E.K. (1979) *Mineralogy of sublimates of Kamchatka volcanoes*. Nauka Publishing House, 152 pp. (in Russian)

Prepublished article

Sheldrick, G.M. (2015) Crystal structure refinement with SHELXL. *Acta Crystallographica*, **C71**(1), 3–8. https://doi.org/10.1107/S2053229614024218

Siidra, O.I., Vergasova, L.P., Kretser, Y.L., Polekhovsky, Y.S., Filatov, S.K. and Krivovichev, S.V. (2014a) Unique thallium mineralization in the fumaroles of Tolbachik Volcano, Kamchatka peninsula, Russia. II. Karpovite, $Tl_2VO(SO_4)_2(H_2O)$. *Mineralogical Magazine*, **78**, 1699-1709. https://doi.org/10.1180/minmag.2014.078.7.13.

Siidra, O.I., Vergasova, L.P., Kretser, Y.L., Polekhovsky, Y.S., Filatov, S.K. and Krivovichev, S.V. (2014b) Unique thallium mineralization in the fumaroles of Tolbachik Volcano, Kamchatka peninsula, Russia. III. Evdokimovite, $Tl_4(VO)_3(SO_4)_5(H_2O)_5$. *Mineralogical Magazine*, **78**, 1711-1724. https://doi.org/10.1180/minmag.2014.078.7.14

Siidra, O.I., Nazarchuk, E.V., Zaitsev, A.N., Lukina, E.A., Avdontseva, E.Y., Vergasova, L.P., Vlasenko, N.S., Filatov, S.K., Turner, R. and Karpov, G.A. (2017) Copper oxosulphates from fumaroles of Tolbachik volcano: puninite, $Na_2Cu_3O(SO_4)_3$ – a new mineral species and structure refinements of kamchatkite and alumoklyuchevskite. *European Journal of Mineralogy*, **29**, 499–510. https://doi.org/10.1127/ejm/2017/0029-2619

Siidra, O.I., Nazarchuk, E.V., Lukina, E.A., Zaitsev, A.N. and Shilovskikh, V.V. (2018) Belousovite, $KZn(SO_4)Cl$, a new sulphate mineral from the Tolbachik volcano with apophyllite sheet-topology. *Mineralogical Magazine*, **82**, 1079–1088. https://doi.org/10.1180/minmag.2017.081.084

Siidra, O.I., Borisov, A.S., Lukina, E., Depmeier W., Platonova N.V., Colmont M. and Nekrasova, D.O. (2019) Reversible hydration/dehydration and thermal expansion of euchlorine, ideally $KNaCu_3O(SO_4)_3$. *Physics and Chemistry of Minerals*, **46**, 403–416. https://doi.org/10.1007/s00269-018-1011-9

Siidra, O.I., Nekrasova, D.O., Charkin, D.O., Zaitsev, A.N., Borisov, A.S., Colmont, M., Mentré, O. and Spiridonova, D.V. (2021) Anhydrous alkali copper sulfates – a promising

Preprinted article

playground for new Cu^{2+} oxide complexes: new Rb-analogues of fumarolic minerals. *Mineralogical Magazine*, **85**, 831-845. doi:10.1180/mgm.2021.73

Vergasova, L.P. and Filatov, S.K. (2012) New mineral species in products of fumarole activity of the great Tolbachik fissure eruption. *Journal of Volcanology and Seismology*, **6**, 281–289. https://doi.org/10.1134/S0742046312050053

Vergasova, L.P. and Filatov, S.K. (2016) A study of volcanogenic exhalation mineralization. *Journal of Volcanology and Seismology*, **10**, 71–85. https://doi.org/10.1134/S0742046316020068

Vergasova, L.P., Filatov, S.K., Serafimova, E.K. and Starova, G.L. (1984) Piypite $K_2Cu_2O(SO_4)_2$ - a new mineral of volcanic sublimates. *Doklady Akademii Nauk SSSR*, **275**, 714–717 (in Russian).

Prepublished article